arXiv:1210.2410v1 [cond-mat.mtrl-sci] 8 Oct 2012

Gain-Driven Discrete Breathers in $\mathcal{PT}-$Symmetric Nonlinear Metamaterials

N. Lazarides[1,2], G. P. Tsironis[1,2]
[1] *Department of Physics, University of Crete, P. O. Box 2208, 71003 Heraklion, Greece;*
[2] *Institute of Electronic Structure and Laser, Foundation for Research and Technology-Hellas, P.O. Box 1527, 71110 Heraklion, Greece*

(Dated: October 10, 2012)

We introduce a one dimensional parity-time ($\mathcal{PT}$)-symmetric nonlinear magnetic metamaterial consisted of split ring dimers having both gain and loss. When nonlinearity is absent we find a transition between an exact to a broken PT-phase; in the former the system features a two band gapped spectrum with shape determined by the gain and loss coefficients as well as the inter-unit coupling. In the presence of nonlinearity we show numerically that as a result of the gain/dissipation matching a novel type of long-lived stable discrete breathers can form below the lower branch of the band with no attenuation. In these localized modes the energy is almost equally partitioned between two adjacent split rings on the one with gain and the other one with loss.

PACS numbers: 63.20.Pw, 11.30.Er, 41.20.-q, 78.67.Pt

Considerable research effort has recently focused in the investigation and developement of artificial materials appropriately engineered to exhibit properties not found in nature. In the electromagnetic domain, these advances resulted in the construction of metamaterials, a class of novel artificial structures that provide full access to all four quadrants of the real permittivity - permeability plane [1]. Recently, there has been increasing interest in synthetic materials that exhibit a combined parity - time ($\mathcal{PT}$) symmetry. Although quantum systems described by $\mathcal{PT}-$symmetric Hamiltonians have been studied for many years [2], the notion of $\mathcal{PT}$ symmetry has now been extended to dynamical lattices, particularly in optics, where $\mathcal{PT}$ related concepts can be realized and tested. Soon after the developement of the theory of $\mathcal{PT}-$symmetric optical lattices [3, 4], the $\mathcal{PT}-$symmetry breaking was experimentally observed [5–7]. Naturally, such considerations have also been extended to nonlinear lattices where the existence of stable discrete solitons [8] and Talbot effects [9] was theoretically demonstrated.

Among many recent developements in $\mathcal{PT}-$symmetric materials, the application of these ideas in electronic circuits [10], not only provides a platform for testing the new ideas within the framework of easily accessible experimental configurations, but also provides a link to the other important class of artifial structures, viz. metamaterials. Magnetic metamaterials, in particular, exhibit high-frequency magnetism and negative permeability in certain frequency intervals [11]. Conventional metamaterials comprising metallic elements suffer from high losses that hamper any possibility for their use in practical applications. However, building metamaterials with $\mathcal{PT}$ symmetry, relying on gain and loss, may provide a way out and moreover lead to new extraordinary properties. It is shown that $\mathcal{PT}-$symmetric metamaterials undergo spontaneous symmetry breaking from the exact $\mathcal{PT}$ phase (real eigenfrequencies) to the broken $\mathcal{PT}$ phase (at least a pair of complex eigenfrequencies), with variation of the gain/loss coefficient. In the presence of nonlinearity, the generation of long-lived nonlinear excitations in the form of discrete breathers (DBs) [12] it is demonstrated numerically in discrete metamaterial models. These novel gain-driven DBs, that may result either by proper intialization of the $\mathcal{PT}$ metamaterial or purely dynamically through external driving, result from power matching of the input power through the gain mechanism and internal loss.

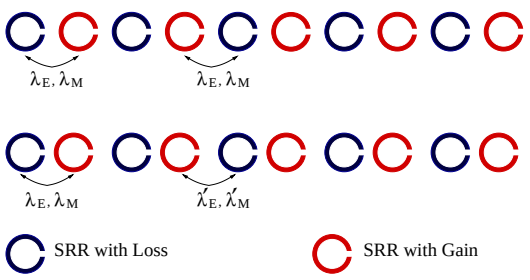


FIG. 1: (Color online) Schematic of a one-dimensional $\mathcal{PT}-$symmetric metamaterial. Upper panel: all the SRRs are equidistant. Lower panel: the separation between SRRs is modulated according to a binary pattern ($\mathcal{PT}$ dimer chain).

Consider a one-dimensional array of periodically arranged dimers, each comprising two split-ring resonators (SRRs); one with loss and the other with equal amount of gain (Fig. 1). The SRRs are coupled magnetically and/or electrically through dipole-dipole forces [13, 14], and are regarded as RLC electrical circuits, featuring a resistance R, an inductance L, and a capacitance C. The SRRs may become nonlinear by the insertion of a varactor diode in their slits [15]. In order to achieve both nonlinearity and gain, a tunnel (Esaki) diode [16] that features a negative resistance part in its current-voltage characteristics can be employed [17]. The incorporation of active constituents in metamaterials that provide gain through external energy sourses has been recognized as a promising technique for compensating losses [18]. Beyond merely

loss compensation, stable metamaterials with net gain have been demonstrated, both as left-handed transmission lines [17] and optical fishnet structures [19].

Within the framework of the equivalent circuit model [14, 20–22], extended for the $\mathcal{PT}-$ dimer chain, the dynamics of the charge q_n accumulated in the capacitor of the $n-$th SRR is governed by

$$\lambda'_M \ddot{q}_{2n} + \ddot{q}_{2n+1} + \lambda_M \ddot{q}_{2n+2} + \lambda'_E q_{2n} + q_{2n+1} + \lambda_E q_{2n+2} = \varepsilon_0 \sin(\Omega\tau) - \alpha q_{2n+1}^2 - \beta q_{2n+1}^3 - \gamma \dot{q}_{2n+1} \quad (1)$$

$$\lambda_M \ddot{q}_{2n-1} + \ddot{q}_{2n} + \lambda'_M \ddot{q}_{2n+1} + \lambda_E q_{2n-1} + q_{2n} + \lambda'_E q_{2n+1} = \varepsilon_0 \sin(\Omega\tau) - \alpha q_{2n}^2 - \beta q_{2n}^3 + \gamma \dot{q}_{2n} \quad (2)$$

where λ_M, λ'_M and λ_E, λ'_E are the magnetic and electric interaction coefficients, respectively, α and β are dimensionless nonlinear coefficients, γ is the gain/loss coefficient ($\gamma > 0$), ε_0 is the amplitude of the external driving voltage, while Ω and τ are the driving frequency and temporal variable, respectively, normalized to the inductive-capacitive (LC) resonance frequency ω_0 and inverse LC resonance frequency ω_0^{-1}, respectively, $\omega_0 = 1/\sqrt{LC_0}$ with C_0 being the linear capacitance. By substituting

$$q_{2n} = Ae^{i(2n\kappa - \Omega\tau)}, \qquad q_{2n+1} = Be^{i((2n+1)\kappa - \Omega\tau)}, \quad (3)$$

where κ is the normalized wavevector, into Eqs. (1) and (2), and requesting nontrivial solutions for the resulting stationary problem, we obtain

$$\Omega_\kappa^2 = \left(-b \pm \sqrt{\Delta}\right)/(2a), \quad (4)$$

where $a = 1 - (\lambda_M - \lambda'_M)^2 - \mu_\kappa \mu'_\kappa$, $b = \gamma^2 - 2\left[1 - (\lambda_E - \lambda'_E)(\lambda_M - \lambda'_M)\right] + \varepsilon_\kappa \mu'_\kappa + \varepsilon'_\kappa \mu_\kappa$, $c = 1 - (\lambda_E - \lambda'_E)^2 - \varepsilon_\kappa \varepsilon'_\kappa$, $\Delta = b^2 - 4ac$, and $\varepsilon_\kappa = 2\lambda_E \cos(\kappa)$, $\varepsilon'_\kappa = 2\lambda'_E \cos(\kappa)$, $\mu_\kappa = 2\lambda_M \cos(\kappa)$, $\mu'_\kappa = 2\lambda'_M \cos(\kappa)$. In the following, we assume that the electric coupling is negligible, i.e., that $\lambda_E = \lambda'_E = 0$, for simplicity. Then, Eq. (4) reduces to

$$\Omega_\kappa^2 = \frac{2 - \gamma^2 \pm \sqrt{\gamma^4 - 2\gamma^2 + (\lambda_M - \lambda'_M)^2 + \mu_\kappa \mu'_\kappa}}{2(1 - (\lambda_M - \lambda'_M)^2 - \mu_\kappa \mu'_\kappa)}. \quad (5)$$

The condition for having real Ω_κ for any κ then reads

$$\cos^2(\kappa) \geq \frac{\gamma^2(2 - \gamma^2) - (\lambda_M - \lambda'_M)^2}{4\lambda_M \lambda'_M}, \quad (6)$$

under the assumption $\lambda_M \lambda'_M > 0$. It is easy to see that for $\lambda_M = \lambda'_M$ the earlier condition cannot be satisfied for all κ's for any positive value of the gain/loss coefficient γ, implying that a large $\mathcal{PT}-$symmetric SRR array (Fig. 1, upper panel) will be in the broken phase. To the contrary, for $\lambda_M \neq \lambda'_M$, i.e., for a periodic dimer chain (Fig. 1, lower panel), the above condition is satisfied for all κ's

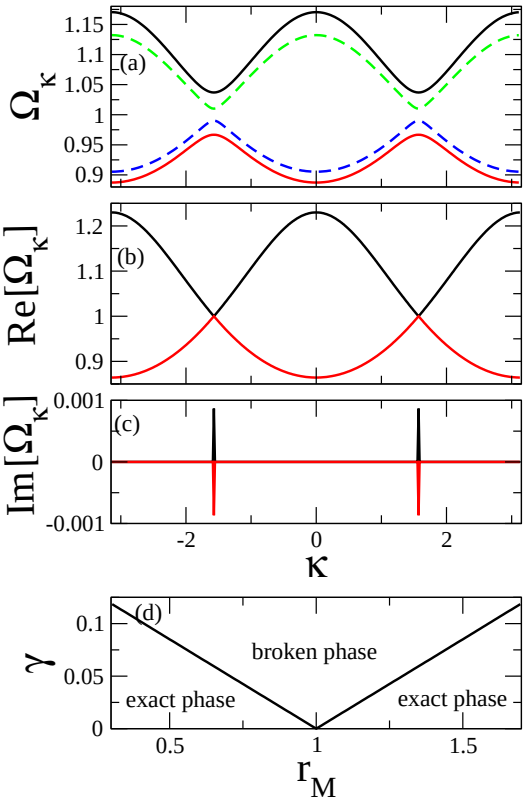


FIG. 2: (Color online) (a) Frequency bands for a $\mathcal{PT}-$symmetric metamaterial with balanced gain and loss ($\gamma = 0.002$) for $\lambda_M = -0.17$ and $\lambda'_M = -0.10$ (black and red solid lines); $\lambda_M = -0.12$ and $\lambda'_M = -0.10$ and (green and blue dashed lines). The imaginary parts are zero (not shown). (b) & (c) Real and imaginary parts, respectively, of the frequency bands for a $\mathcal{PT}-$symmetric metamaterial with balanced gain and loss ($\gamma = 0.002$) for $\lambda_M = -0.17$ and $\lambda'_M = -0.1699$. (d) The boundary between the exact and the broken phase on the $\gamma - r_M$ plane, where $r_M = \lambda'_M/\lambda_M$, for $\lambda_M = -0.17$.

for $\gamma \leq \gamma_c \simeq |\lambda_M - \lambda'_M|$, ($\gamma^4 \simeq 0$). In the exact phase ($\gamma < \gamma_c$), the $\mathcal{PT}-$symmetric dimer array has a gapped spectrum with two frequency bands (Fig 2a). The width of the gap separating the bands decreases with decreasing $|\lambda_M - \lambda'_M|$ for constant γ. For $\gamma \simeq \gamma_c$ the gap closes (Fig. 2b), some frequencies in the spectrum acquire an imaginary part as shown in Fig. 2c, and the $\mathcal{PT}$ metamaterial goes into the broken phase. The two phases are separated by the exceptional point $\gamma = \gamma_c$, which varies with the other parameters. A typical phase diagram on the $\gamma - r_M$ plane, with $r_M = \lambda'_M/\lambda_M$ is shown in Fig. 2d. For fixed λ_M, λ'_M, the bandwidths as a function of γ are shown in Fig. 3.

Eqs. (1) and (2) implemented by $q_0(\tau) = q_{N+1}(\tau) = 0$ that accounts for the termination of the structure in finite systems, are integrated numerically with initial condition

$$q_m(0) = (-1)^{m-1}\mathrm{sech}(m/2), \qquad \dot{q}_m(0) = 0, \quad (7)$$

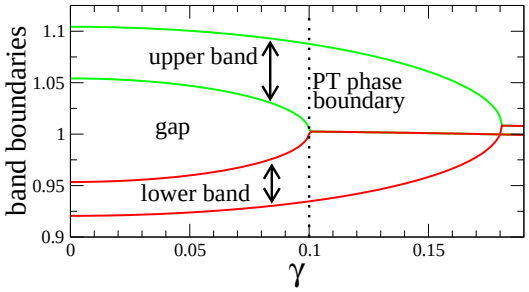


FIG. 3: (Color online) Frequency bands boundaries as a function of the gain/loss parameter γ for a $\mathcal{PT}-$symmetric metamaterial with balanced gain and loss in the dimer array configuration, for $\lambda_M = -0.14$, and $\lambda'_M = -0.04$.

$\varepsilon_0 = 0$, and nonlinear coefficients $\alpha = -0.4$, $\beta = 0.08$. Using a gain/loss function of the form

$$\gamma(m) = \begin{cases} \gamma, & m = 1, ..., N_\ell \\ (-1)^{m-1}\gamma, & m = N_\ell + 1, ..., N - N_\ell \\ \gamma, & m = N - N_\ell + 1, ..., N, \end{cases} \qquad (8)$$

we obtain gain-driven DBs that remain stable for very long times ($> 10^8$ time units) for relatively wide parameter intervals. Note that the actual $\mathcal{PT}-$symmetric dimer chain is of length $N - 2N_\ell$, while both its ends are joined to lossy dimer chains of length N_ℓ. We found empirically that this is the most effective way to stabilize DBs in the $\mathcal{PT}$ metamaterial, i.e., by embedding it into a lossy metamaterial. The lossy parts help the excess energy to go smothly away during the long transient phase of integration, and thus prevents the blowing up of the solution that otherwise may have occured. Fig. 4 shows typical examples of the energy density evolution of a breather excitation in the $n - \tau$ plane. The largest part of the total energy is concentrated into two neighboring sites belonging to the same gain/loss dimer. The corresponding instantaneous current profiles i_n as a function of n at maximum current are shown in Fig. 5. Note that these profiles are neither symmetric or antisymmetric at the SRR level.

The breather oscillation frequency Ω_B can be obtained from the power spectrum of a time series of the energy in one of the breather sites. Such a typical power spectrum is shown in Fig. 6a, where the logarithm of the power spectrum is plotted as a function of frequency; strong harmonics to the fundamental frequency Ω_B are clearly observed. The frequency Ω_B increases with decreasing $|\lambda_M - \lambda'_M|$ as can be seen in Fig. 6b, while the variation of the gain/loss coefficient γ within $10^{-2} - 10^{-3}$ has apparently no effect on Ω_B at least in the particular case shown in Fig. 6c. The dependence of Ω_B on $|\lambda_M - \lambda'_M|$ is illustrated in Fig. 6d, for those values of $|\lambda_M - \lambda'_M|$ for which DB excitations are stable (or at least long-lived).

For a gapped linear spectrum, large amplitude linear modes become unstable in the presence of driving and

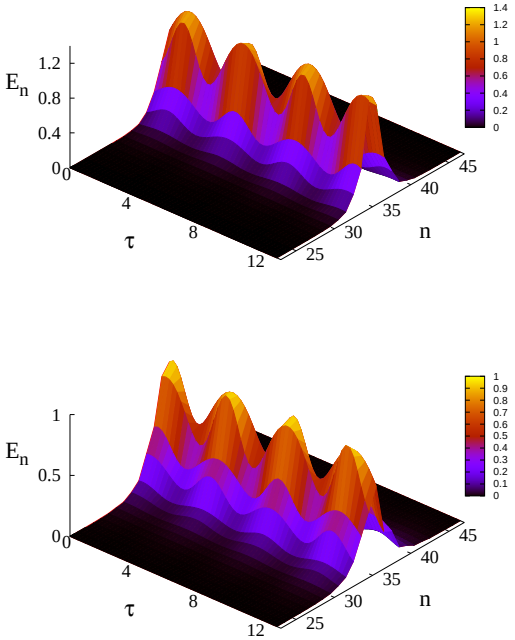


FIG. 4: (Color online) Spatiotemporal evolution of the energy density E_n for approximatelly two $LC-$ periods for $N = 70$, $N_\ell = 10$, $\lambda'_M = -0.10$, $\lambda_E = \lambda'_E = 0$, $\gamma = 0.002$, and (upper panel) $\lambda_M = -0.17$; (lower panel) $\lambda_M = -0.21$. Energy localization at two neighboring sites, one with gain and one with loss, is clearly observed. Only part of the array is shown for clarity.

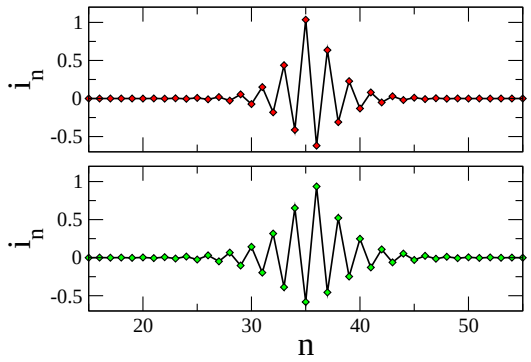


FIG. 5: (Color online) Gain-driven, current breather instantaneous profiles i_n as a function of n at maximum current amplitude, for $N = 70$, $N_\ell = 10$, $\lambda'_M = -0.10$, $\lambda_E = \lambda'_E = 0$, $\gamma = 0.002$, and (a) $\lambda_M = -0.17$; (b) $\lambda_M = -0.21$. Only part of the array is shown for clarity.

nonlinearity. If the curvature of the dispersion curve in the region of such a mode is positive and the lattice potential is soft, large amplitude modes become unstable with respect to formation of DBs in the gap below the linear spectrum [23]. For the parameters of Fig. 2a, the bottom of the lower band is located at $\Omega_0 \simeq 0.887$, where

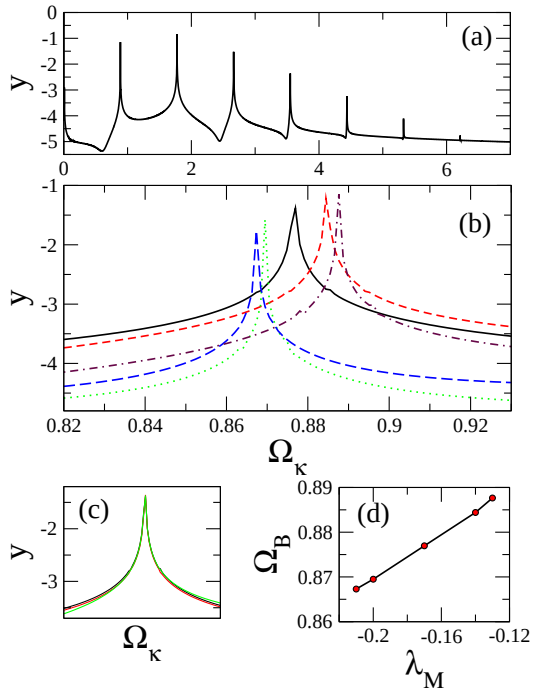


FIG. 6: (Color online) (a) The logarithm of the power spectrum of energy at one of the central breather sites $y = log_{10}[PS(E_{n=N/2})]$ is shown as a function of the frequency Ω_κ, for $N = 70$, $\lambda'_M = -0.10$, $\lambda_M = -0.13$, $\lambda_E = \lambda'_E = 0$, $\gamma = 0.002$. (b) The same as in (a) around the fundamental breather frequency Ω_B, for $\lambda_M = -0.21$ (blue - long dashed); $\lambda_M = -0.20$ (green - dotted); $\lambda_M = -0.17$ (black - solid); $\lambda_M = -0.14$ (red - dashed); $\lambda_M = -0.13$ (maroon - dotted dashed). The other parameters as in (a). (c) The same as in (a) and (b) around the fundamental breather frequency Ω_B, for three different values of the gain/loss coefficient γ: 0.002 (black); 0.005 (green); 0.01 (red). (d) Dependence of Ω_B on the magnetic coupling coefficient λ_M, for the spectra shown in (b).

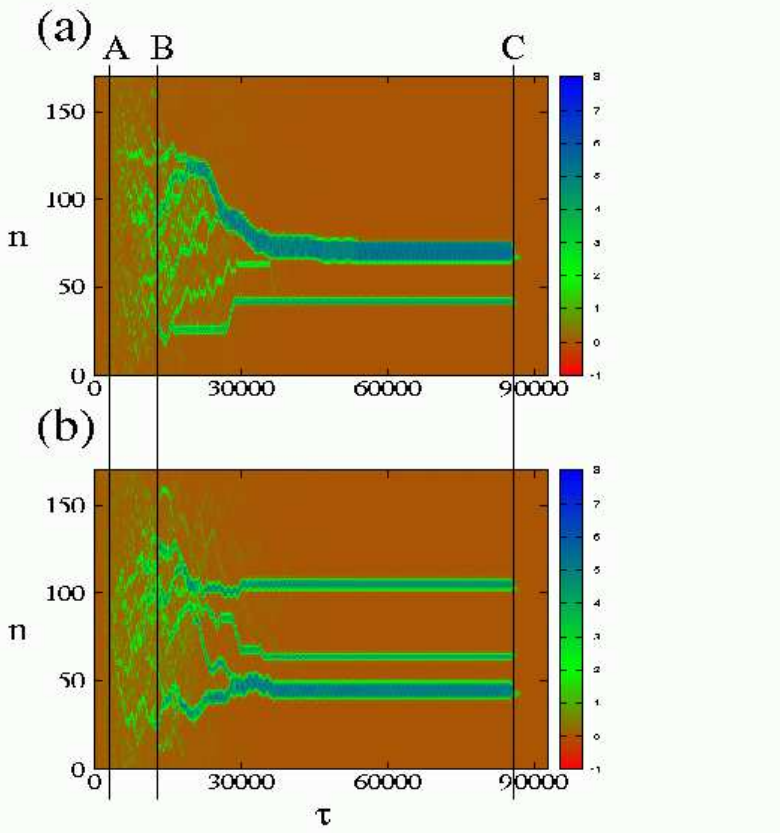


FIG. 7: (Color online) Spatiotemporal evolution of the energy density E_n for a $\mathcal{PT}-$symmetric dimer chain with $N = 70$, $N_\ell = 10$, $\Omega_0 = 0.887$, $\gamma = 0.002$, $\lambda_M = -0.17$, $\lambda'_M = -0.10$ ($\lambda_E = \lambda'_E = 0$), and (a) $\varepsilon_0 = 0.085$; (b) $\varepsilon_0 = 0.095$. The vertical lines separate different stages in the chirping procedure (see text).

the curvature is positive. Moreover, the SRRs are subjected to soft on-site potentials for the selected values of the nonlinear coefficients α and β. Then, DBs can be generated spontaneously by a frequency chirped driver as it is illustrated in Fig. 7, where the evolution of the energy density E_n for a $\mathcal{PT}-$symmetric dimer chain is plotted on the $n - \tau$ plane. We use the following procedure: At time $\tau = 0$, we start integrating Eqs. (1) and (2) with zero initial state and external driving for 500 $T_0 \simeq 3500$ time units (t.u.), where $T_0 = 2\pi/\Omega_0$, to allow for significant developement of large amplitude modes. At time $\tau \simeq 3500$ t.u. (point A on Fig. 7), the driver is switched-on with low-amplitude and frequency slightly above Ω_0 ($1.01\ \Omega_0 \simeq 0.894$). The frequency is then chirped downwards with time to induce instability for the next $10,600$ t.u. ($\sim 1500\ T_0$), until it is well below Ω_0 ($0.997\ \Omega_0 \simeq 0.882$). During that phase, a large number of excitations are generated that move and strongly interact to each other, eventually merging into a small number of high amplitude (multi-)breathers. At time $\tau \simeq 14,100$ t.u. (point B on Fig. 7), the driver is switched off and the DBs that have formed are solely driven by the gain. They continue to interact until they reach a stationary state and get trapped at particular sites. The high density segments between points B and C in Fig. 7 present precisely those stationary gain-driven breathers and multibreathers generated through chirping and subsequent dynamics. At time $\tau \sim 85150$ t.u. (point C on Fig. 7), the gain is replaced by equal amount of loss, and the breathers die out rapidly.

The construction of metamaterial elements with gain is nowadays feasible. In the microwave frequency range, in particular, the use of negative resistance devices like tunnel diodes [17, 24] and transistors [25] seems to be very convinient for providing gain in transmission lines and SRRs. Thus, a stable $\mathcal{PT}$ metamaterial whose dynamics is approximatelly described by model equations like (1) and (2) can be realized and tested. In the specific case of a balanced configuration, where dissipation is counterbalanced by equal amount of gain, it is demonstrated numer-

ically that stable or at least long-lived, gain-driven DBs may be generated. DB generation can be achieved either by proper initialization of the system, or purely dynamically by frequency chirping of a weak alternating driving applied homogeneously to all elements of the dimer chain. Importantly, single-site DBs apparently cannot be formed but instead, fundamental breather excitations occupy two neighboring sites, one with gain and the other with loss, belonging to the same dimer. Stabilization of these localized modes can be achieved by embedding the $\mathcal{PT}-$symmetric dimer chain into a lossy dimer chain, as it was found empirically. It is also worth mentioning that in a slightly unbalanced configuration, where absolute gain and loss differ by a small amount, DBs may still be generated through the chirping dynamical procedure that are not stable in the long term. When loss exceeds gain, the generated DBs decay slowly until they vanish in a time-scale proportional to the gain/loss imbalance. In the opposite case, the DBs gain energy in the course of time becoming wider while in the long term their energy diverges.

This work was supported by the "THALES" Project ANEMOS, funded by the ESPA Program of the Ministry of Education of Greece.

[1] N. I. Zheludev, Science **328**, 582 (2010), and refs therein.
[2] D. W. Hook, Ann. Phys. (Berlin) **524 (6-7)**, A106 (2012), and references therein.
[3] R. El-Ganainy, K. G. Makris, D. N. Christodoulides, and Z. H. Musslimani, Opt. Lett. **32**, 2632 (2007).
[4] K. G. Makris, R. El-Ganainy, D. N. Christodoulides, and Z. H. Musslimani, Phys. Rev. Lett. **100**, 103904 (2008).
[5] A. Guo *et al.*, Phys. Rev. Lett. **103**, 093902 (2009).
[6] C. E. Rüter *et al.*, Nature Physics **6**, 192 (2010).
[7] A. Szameit, M. C. Rechtsman, O. Bahat-Treidel, and M. Segev, Phys. Rev. **A 84**, 021806(R) (2011).
[8] S. V. Dmitriev, A. A. Sukhorukov, and Yu. S. Kivshar, Opt. Lett. **35**, 2976 (2010).
[9] H. Ramezani, D. N. Christodoulides, V. Kovanis, I. Vitebskiy, and T. Kottos, Phys. Rev. Lett. **109**, 033902 (2012).
[10] J. Schindler, Ang Li, M. C. Zheng, F. M. Ellis, and T. Kottos, Phys. Rev. A **84**, 040101(R) (2011).
[11] S. Linden *et al.*, IEEE J. Selec. Top. Quant. Electron. **12**, 1097 (2006).
[12] S. Flach and A. V. Gorbach, Phys. Rep. **467**, 1 (2008).
[13] I. Sersić, M. Frimmer, E. Verhagen, and A. F. Koenderink, Phys. Rev. Lett. 103, 213902 (2009).
[14] N. N. Rosanov *et al.*, Opt. Express **19**, 26500 (2011).
[15] B. Wang, J. Zhou, T. Koschny, and C. M. Soukoulis, Opt. Express **16**, 16058 (2008).
[16] L. Esaki, Phys. Rev. **109**, 603 (1958).
[17] T. Jiang, K. Chang, L.-M. Si, L. Ran, and H. Xin, Phys. Rev. Lett. **107**, 205503 (2011).
[18] A. D. Boardman *et al.*, Laser Photonics Rev. **5**, 287 (2010).
[19] S. Xiao *et al.*, Nature **466**, 735 (2010).
[20] N. Lazarides, M. Eleftheriou, and G. P. Tsironis, Phys. Rev. Lett. **97**, 157406 (2006).
[21] M. I. Molina, N. Lazarides, and G. P. Tsironis, Phys. Rev. E **80**, 046605 (2009).
[22] N. Lazarides, V. Paltoglou, and G. P. Tsironis, Int. J. Bifurcation Chaos **21**, 2147 (2011).
[23] M. Sato *et al.*, Phys. Rev. Lett. **90**, 044102 (2003).
[24] A. D. Boardman, Yu. G. Rapoport, N. King, and V. N. Malnev, J. Opt. Soc. Am. B **24**, A53-A61 (2007).
[25] W. Xu, W. J. Padilla, and S. Sonkusale, arXiv:1204.6067v1 [physics.optics] .